

## Studies of $\Upsilon(1S)$ state production with the DØ Detector at Fermilab

The DØ Collaboration  
URL <http://www-d0.fnal.gov>  
(Dated: August 2, 2004)

We present a preliminary measurement of the inclusive production cross section of the  $\Upsilon(1S)$  bottomonium state using the  $\Upsilon(1S) \rightarrow \mu^+ \mu^-$  decay mode. The data sample corresponds to an integrated luminosity of  $159.1 \pm 10.3 \text{ pb}^{-1}$ . We determine differential cross sections as functions of the  $\Upsilon(1S)$  transverse momentum,  $p_T^\Upsilon$ , for three ranges of the  $\Upsilon(1S)$  rapidity:  $0 < |y^\Upsilon| < 0.6$ ,  $0.6 < |y^\Upsilon| < 1.2$ , and  $1.2 < |y^\Upsilon| < 1.8$ . The shapes of  $d\sigma/dp_T$  cross sections show little variation with rapidity and are consistent with the published Run I CDF measurement over the rapidity range  $|y^\Upsilon| < 0.4$ . The absolute cross sections integrated over  $p_T$  are also consistent with the previous measurements and exhibit rapidity dependence as expected from Monte Carlo.

## I. PHYSICS MOTIVATION

Quarkonium production provides insight into the nature of strong interactions. It is a window on the boundary region between perturbative and non-perturbative QCD. Recent advances in the understanding of quarkonium production have been stimulated by the unexpectedly large cross sections for direct  $J/\psi$  and  $\psi(2S)$  production at large  $p_T$  measured at the Fermilab Tevatron [1]. Three types of models have been used to describe the quarkonium formation: the color-singlet model [2]; the color-evaporation model [3] (and a follow up soft color interaction model [4]); and the color-octet model [5]. In the color-singlet model, the charmonium meson retains the quantum numbers of the produced  $c\bar{c}$  ( $b\bar{b}$ ) pair, and thus each  $J^{PC}$  state can only be directly produced via the corresponding hard scattering color-singlet sub-processes. In the color-evaporation model, the directly produced charmonium meson is not constrained to the same  $J^{PC}$  state as the  $c\bar{c}$  ( $b\bar{b}$ ) pair produced in the hard scatter because of the emission of soft gluons during the meson's formation. The color-octet mechanism extends the color-singlet approach by taking into account the production of  $c\bar{c}$  ( $b\bar{b}$ ) pairs in a color-octet configuration. The color-octet state evolves into a color-singlet state via emission of soft gluons. These models of quarkonium formation lead to different expectations for the production rates and polarization of the quarkonium states.

A very recent paper [6] successfully reproduces the transverse momentum distribution of upsilon states produced at Tevatron energies by combining separate perturbative approaches for low- and high- $p_T$  regions. However, several model parameters have been adjusted to match the data, and the absolute cross section is not predicted by these calculations.

In this note we concentrate on the production of the bottomonium state  $\Upsilon(1S)$ . Contrary to the charmonium state production, there is no contribution from the  $b$  quark decays. Hence, bottomonium states are expected to be produced promptly, i.e. at the primary vertex, and to be relatively isolated in space from other interaction products. However, a fraction of  $\Upsilon(nS)$  mesons are produced indirectly, as a result of a decay of a higher mass state, e.g., a radiative decay  $\chi_b \rightarrow \Upsilon(1S)\gamma$  or  $\Upsilon(2S) \rightarrow \Upsilon(1S)\pi\pi$ .

The only detailed studies of the  $\Upsilon(nS)$  production at the Tevatron, based on the Run I data, were done by the CDF Collaboration[7–9]. The most important of the CDF findings are: (i) inclusive cross sections for  $\Upsilon(nS)$  states in the rapidity range  $|y^\Upsilon| < 0.4$  are in excess of the predictions of the color-singlet model by more than an order of magnitude for  $p_T^\Upsilon > 10$  GeV/c [10], (ii) approximately 50% of  $\Upsilon(1S)$  mesons are produced directly, and (iii)  $\Upsilon(1S)$  polarization for  $8 < p_T^\Upsilon < 20$  GeV/c is  $\alpha = -0.12 \pm 0.22$ .

The parameter  $\alpha = 1(-1)$  corresponds to 100% transverse (longitudinal)  $\Upsilon(1S)$  polarization. This result is consistent with the prediction of the color-octet model [11]. The model also predicts a steady increase of transverse polarization with transverse momentum (due to the contribution from gluon fragmentation) and a much larger polarization for more massive bottomonium states  $\Upsilon(2S)$  and  $\Upsilon(3S)$ , which are produced more directly than  $\Upsilon(1S)$ .

A much larger transverse polarization for  $\Upsilon(2S)$  and  $\Upsilon(3S)$  than for  $\Upsilon(1S)$  has also recently been observed in bottomonium production in the p-Cu collisions at  $\sqrt{s} = 38.8$  GeV by the Fermilab E866/NuSea Collaboration [12]. For a recent review of the experimental results on quarkonium production in Run I as well as from other relevant experiments, see Ref. [13].

## II. DATA

In this study, we determine the production cross section of  $\Upsilon(1S)$  as a function of its transverse momentum, in three rapidity ranges:  $0 < |y^\Upsilon| < 0.6$ ,  $0.6 < |y^\Upsilon| < 1.2$ , and  $1.2 < |y^\Upsilon| < 1.8$ .

The data were collected between June 2002 and September 2003 using a scintillator based dimuon triggers at Level 1 and a loose confirmation of a muon presence at Level 2. The Level 1 trigger is approximately fully efficient for muons with transverse momentum of 5 GeV/c. The Level 2 trigger requirement kept more than 97% of events which satisfied Level 1. The triggers ran unprescaled during the time period covered by this analysis. After removing corrupted data the integrated luminosity of the sample was found to be  $159.1 \pm 10.3$  pb<sup>-1</sup> (we assume a standard DØ 6.5% luminosity uncertainty).

The analysis requires two opposite-charge muon candidates, with wire hits inside and outside the toroid magnets, and with each candidate matched to a central track. Kinematic cuts on the muon candidates are:  $p_T^\mu > 3$  GeV/c, and  $|\eta^\mu| < 2.2$ . We also require that the central track associated with a muon candidate had at least one SMT hit, and satisfied the muon cosmic rejection cut. We expect the upsilon states to be *isolated*. We define our upsilon isolation requirement as at least one muon satisfying either: (i) a sum of transverse energies of charged tracks in a cone of radius 0.5 (in the  $\eta - \phi$  space) around the muon less than  $< 1$  GeV, or, (ii) a sum of the calorimeter transverse energies in an annulus cone of radii 0.1 and 0.5 around the muon less than  $< 1$  GeV. This isolation requirement reduces the background by 35% and the signal by less than 6%. It is applied to allow a better separation of the  $\Upsilon(1S)$  signal,

however, its efficiency has to be derived from the data. An additional requirement on the isolation of the upilon candidate itself does not improve the signal to background ratio significantly, and has not been applied.

There are 353k oposite charge muon pairs with invariant mass in the 7 - 13 GeV $c^2$  range left in the sample. Several examples of dimuon mass plots are shown in Fig. 1. In each plot a strong  $\Upsilon(1S)$  signal is shown accompanied by a shoulder representing unresolved signals due to  $\Upsilon(2S)$  and  $\Upsilon(3S)$  production.

The mass distributions were fitted in the 7.0 (7.8)–13.0 GeV range using three mass resolution functions for each of the  $\Upsilon(nS)$  bound states and a third order polynomial for the background. The mass resolution function was approximated by a sum of two Gaussians with the relative contribution and the width of the second Gaussian fixed, based on Monte Carlo studies and  $J/\psi$  signal fits in the data. The measured mass of  $\Upsilon(1S)$  was a free parameter of the fit, the remaining two masses were shifted by the  $m(\Upsilon(nS)) - m(\Upsilon(1S))$  differences of 563 MeV/ $c^2$  ( $\Upsilon(2S)$ ) and 840 MeV/ $c^2$  ( $\Upsilon(3S)$ ), taken from the Ref [14]. In addition, only the width of the  $\Upsilon(1S)$  state,  $\sigma(\Upsilon(1S))$ , was allowed to vary. The width of the other states were assumed to scale with the mass of the resonance. Normalizations of resolution functions representing each resonance were free parameters of the fit.

Approximately 200k  $\Upsilon(1S)$  Monte Carlo events, generated with the PYTHIA [15] generator v6.202, were processed through the detector and trigger simulator and the DØ off-line reconstruction program. We have verified that the muon kinematic distributions from data and Monte Carlo, plotted in restricted regions of  $p_T^{\Upsilon}$  and  $y_T^{\Upsilon}$ , agree quite well.

### III. CROSS SECTION CALCULATIONS

The cross section for a given kinematic range, multiplied by the branching ratio  $\Upsilon(1S) \rightarrow \mu^+\mu^-$ , is given by:

$$\frac{d^2\sigma(\Upsilon(1S))}{dp_T \cdot dy} = \frac{N(\Upsilon)}{\mathcal{L} \cdot \Delta p_T \cdot \Delta y \cdot \varepsilon_{kinem} \cdot \varepsilon_{acc} \cdot \varepsilon_{trigg-reco} \cdot \varepsilon_{iso-SMT} \cdot \varepsilon_{dimu} \cdot \varepsilon_{trk} \cdot \varepsilon_{fit}} \quad (1)$$

where  $\mathcal{L}$  is the integrated luminosity for the data sample used,  $N(\Upsilon(1S))$  is the number of observed (fitted)  $\Upsilon(1S)$  events, and  $\varepsilon_i$  represent various efficiency and acceptance factors.

The muon acceptance and reconstruction efficiency is based on Monte Carlo analysis and has been factorized into two parts: losses due to kinematic cuts on muon momenta before the Monte Carlo events were processed through the simulation/reconstruction packages ( $\varepsilon_{kinem}$ ), and an acceptance/reconstruction efficiency for muons that passed the kinematic cut ( $\varepsilon_{acc}$ ). The product ( $\varepsilon_{kinem} \cdot \varepsilon_{acc}$ ) represents a fraction of generated  $\Upsilon(1S)$  candidates that was successfully reconstructed in the DØ detector, without the trigger condition imposed. The dimuon trigger efficiency ( $\varepsilon_{trigg-reco}$ ) for reconstructed dimuons was estimated by running a trigger simulator and verified directly with the data using other triggers. The remaining factors in Eq.1 account for the differences between the data and Monte Carlo efficiencies.

The correction ( $\varepsilon_{iso-SMT}$ ) is defined as a ratio of the number of fitted upilon candidates obtained with and without the data quality cuts (isolation, SMT-hit requirement, cosmic rejection), divided by the corresponding ratio of the Monte Carlo  $\varepsilon_{acc} \cdot \varepsilon_{trigg}$  efficiencies for these two cases. It was derived from the data. It is consistent with being  $p_T$  independent at its numerical values vary between 0.85 and 0.93 as a function of rapidity.

The central track matching correction ( $\varepsilon_{trk}$ ) was derived from the  $J/\psi$  data and Monte Carlo and turns out to be very close to unity except for the forward rapidity region where  $\varepsilon_{trk} \approx 0.95$ .

The correction factor ( $\varepsilon_{dimu}$ ) accounts for both the differences in the *local* muon reconstruction and trigger efficiencies between data and Monte Carlo. The data-Monte Carlo correction for individual muons was determined using muons from  $J/\psi$  events collected with single muon triggers. It does not show a significant  $p_T$  dependence, but it changes with the muon pseudorapidity. It is close to unity for muons with  $|\eta^\mu| < 0.3$  and  $|\eta^\mu| > 1.1$ . It drops to  $\approx 0.9$  in the intermediate region between central and forward muon detectors. Correction  $\varepsilon_{dimu}$  was derived by propagating corrections for individual muons using Monte Carlo. The trigger inefficiency contribution to the  $\varepsilon_{dimu}$  correction was verified using relative single- and di-muon trigger efficiencies for the  $\Upsilon(1S)$  events from the data.

### IV. RESULTS

In Table I we summarize typical values of efficiencies applied in different rapidity regions. Figure 2 shows the dependence of the overall Monte Carlo derived efficiency on transverse momentum. A minimum of the efficiency at intermediate  $p_T$  values is understood as a result of changes in topologies for events accepted by the DØ detector. Efficiencies shown in Fig. 2 do not contain data-derived corrections  $\varepsilon_{iso-SMT}$ ,  $\varepsilon_{dimu}$ , and  $\varepsilon_{trk}$ .

Calculated cross sections are collected in Table II. The cross sections are normalized per unit of rapidity. Cross sections for the  $|y^\Upsilon| < 1.8$  range were determined in parallel with those for smaller rapidity bins, with every step done

separately, including mass fits. Therefore, the fitted number of events for that region does not need to be exactly equal to the sum of signal events fitted in smaller rapidity bins.

TABLE I: Typical efficiencies used for the cross section calculations.

$ y^\Upsilon $	$\epsilon_{kinem}$	$\epsilon_{acc}$	$\epsilon_{trig,eco}$	$\epsilon_{trk}$	$\epsilon_{dimu}$	$\epsilon_{fit}$	$\epsilon_{iso-SMT}$
0.0 - 0.6	0.5 - 0.7	0.3 - 0.4	0.70	0.99	0.85	1.0	0.85
0.6 - 1.2	0.5 - 0.7	0.4 - 0.5	0.73	0.99	0.88	1.0	0.85
1.2 - 1.8	0.4 - 0.6	0.5 - 0.6	0.82	0.95	0.95	1.0	0.93

The measured cross section times  $BR(\Upsilon(1S) \rightarrow \mu^+\mu^-)$  for the  $|y^\Upsilon| < 0.6$  region is  $749 \pm 20(stat) \pm 75(syst) \pm 49(luminosity)$  pb and is compatible with the CDF Run I result of  $680 \pm 15(stat) \pm 18(syst) \pm 26(luminosity)$  pb for the  $\sqrt{s} = 1.8$  TeV (we derived this value from the information provided in Ref. [9]). The cross sections are expected to increase by 11% (PYTHIA Monte Carlo) when the  $p\bar{p}$  center-of-mass energy increases from 1.8 TeV to 1.96 TeV.

TABLE II: Fitted number of events with the SMT hit and isolation requirements. Integrated  $\Upsilon(1S)$  cross sections per unit of rapidity.

$ y^\Upsilon $	Number of $\Upsilon(1S)$ candidates SMT+Isolation req.	Total cross section (pb) <i>stat (syst)</i>
0.0 - 0.6	13,040	$749 \pm 20(stat) \pm 75(syst)$
0.6 - 1.2	16,867	$781 \pm 21(stat) \pm 78(syst)$
1.2 - 1.8	18,122	$598 \pm 19(stat) \pm 56(syst)$
0.0 - 1.8	46,331	$695 \pm 12(stat) \pm 65(syst)$

Differential cross sections, normalized to unity, are summarized in Table III and plotted in Fig. 3.

There is little variation in the shape of  $p_T$  distributions with rapidity. As seen from Figure 4, our combined differential cross section for  $|y^\Upsilon| < 1.8$  is consistent with the Run I CDF measurement in the limited rapidity range of  $|y^\Upsilon| < 0.4$  [9].

The cross sections integrated over  $p_T$  are shown in Fig.5 as functions of  $|y^\Upsilon|$ . We find the ratios of cross sections of the  $0.6 < |y^\Upsilon| < 1.2$  and  $1.2 < |y^\Upsilon| < 1.8$  ranges to that for the  $|y^\Upsilon| < 0.6$  bin to be:  $1.04 \pm 0.14$  and  $0.80 \pm 0.11$ , respectively. These values are consistent with the PYTHIA Monte Carlo predictions of 0.94 and 0.83, respectively.

Finally, the ratios of differential cross section for different pairs of rapidity bins are shown in Fig. 6. The systematic uncertainties in the relative normalizations are also indicated.

TABLE III: Normalized differential cross sections in  $(GeV/c)^{-1}$  for  $\Upsilon(1S)$  in different rapidity regions. Quoted uncertainties include uncertainties due to the assumed shape of the mass resolution function.

$p_T^\Upsilon (GeV/c)^{-1}$	$0.0 <  y^\Upsilon  < 0.6$	$0.6 <  y^\Upsilon  < 1.2$	$1.2 <  y^\Upsilon  < 1.8$	$0.0 <  y^\Upsilon  < 1.8$
0 - 1	$0.050 \pm 0.005$	$0.061 \pm 0.006$	$0.053 \pm 0.005$	$0.057 \pm 0.004$
1 - 2	$0.137 \pm 0.009$	$0.138 \pm 0.010$	$0.135 \pm 0.011$	$0.125 \pm 0.006$
2 - 3	$0.153 \pm 0.010$	$0.153 \pm 0.010$	$0.172 \pm 0.015$	$0.160 \pm 0.008$
3 - 4	$0.148 \pm 0.011$	$0.175 \pm 0.012$	$0.166 \pm 0.013$	$0.163 \pm 0.008$
4 - 6	$0.112 \pm 0.007$	$0.110 \pm 0.007$	$0.115 \pm 0.007$	$0.115 \pm 0.005$
6 - 8	$0.067 \pm 0.005$	$0.061 \pm 0.004$	$0.054 \pm 0.005$	$0.063 \pm 0.003$
8 - 10	$0.035 \pm 0.003$	$0.034 \pm 0.003$	$0.035 \pm 0.003$	$0.036 \pm 0.002$
10 - 15	$0.0137 \pm 0.001$	$0.0107 \pm 0.0009$	$0.0110 \pm 0.001$	$0.0118 \pm 0.0006$
15 - 20	$0.0029 \pm 0.0005$	$0.0019 \pm 0.0003$	$0.0016 \pm 0.0003$	$0.00215 \pm 0.0002$

The overall systematic uncertainties, as discussed in the next section, are approximately 10%.

## V. SYSTEMATICS

In this analysis we are concerned with systematic uncertainties that are  $p_T$  dependent and with those that are common and affect the absolute normalization of the cross sections. We estimated the effects of the mass resolution

TABLE IV: Dominant systematic uncertainties.

Source	$0.0 <  y^{\Upsilon}  < 0.6$	$0.6 <  y^{\Upsilon}  < 1.2$	$1.2 <  y^{\Upsilon}  < 1.8$
Luminosity	6.5%	6.5%	6.5%
fitting procedure	3.0%	4.0%	4.0%
isolation, SMT hit requir.	2.0%	2.0%	1.7%
MC kinematic properties	<2.0%	<2.0%	<2.0%
momentum resolution	<1%	<1%	<1%
central track matching	2.0%	2.0%	3.0%
local $\mu$ ID and trigger	8.7%	8.2%	7.2%
detector performance vs time	2.0%	2.0%	2.0%
TOTAL (no lum, polar)	10.0%	10.0%	9.4%

function uncertainty on the fit bin-to-bin variations by doubling the contribution of the second Gaussian. Next, the difference in the number of fitted  $\Upsilon(1S)$  candidates was added in quadrature to the regular fit uncertainties. The net effect is an increase in the overall fit uncertainty by less than 40% of its value.

The remaining systematic uncertainties have a minimal effect on the  $\Upsilon(1S)$   $p_T$  distributions. Several common systematic uncertainties have been identified that are not included in the normalized cross section error bars shown in Fig. 3.

(i) The nominal uncertainty for the luminosity is 6.5%.

(ii) The kinematic (pre-Geant) efficiencies,  $\varepsilon_{kinem}$ , were obtained by varying the hard scatter  $PTLOW$  parameter in PYTHIA and are found negligible.

(iii) Common systematic uncertainties of  $\varepsilon_{fit}$  were estimated from: (a) a comparison of numbers of fitted events with the resolution function width either treated as a fit parameter or fixed, and from variations in the mass fit range, (b) number of events obtained using either single- or double-Gaussian resolution functions, and (c) varying the mass fit range by  $\pm 0.2$  GeV.

(iv) Systematic uncertainties of  $\varepsilon_{iso-SMT}$  were estimated from the mass fits for the combined  $\Upsilon(nS)$  signal, with and without muon quality requirements.

(v) The uncertainty of the  $\varepsilon_{acc}$  efficiency was obtained by reweighting Monte Carlo events so that they match  $\Upsilon(1S)$  differential cross sections determined in the first pass. The only significant change of efficiency was observed for the last two, 5 GeV/c wide,  $p_T$  bins, and it was less than 3%.

(vi) The largest contribution to systematic uncertainty is due to  $\varepsilon_{dimu}$ , representing the differences between the local muon ID and trigger efficiencies obtained from data and Monte Carlo. This systematic uncertainty reflects: (a) limited statistics of the control data and Monte Carlo samples, (b) variations in the conditions under which these corrections were studied, such as: selection cuts for the trigger and test muons,  $J/\psi$  signal fits, composition of the  $J/\psi$  Monte Carlo, detector symmetries etc. Statistical and systematic uncertainties, determined as functions of kinematic variables describing individual muons were added in quadrature and propagated into uncertainty for  $\varepsilon_{dimu}$  using Monte Carlo. Our conservative estimates for these uncertainties are: 8.7, 8.2, and 7.2% for the three rapidity bins, respectively.

(vii) The uncertainty of  $\varepsilon_{trk}$ , the track matching data-Monte Carlo correction, contributes less than 2%.

(viii) Uncertainty due to the finite momentum resolution was estimated by comparing the numbers of reconstructed Monte Carlo events, assigned to a given  $\Upsilon(1S)$  kinematic bin, with either original or smeared muon momenta used.

(ix) Uncertainties due to variations in the detector performance were studied by plotting number of signal events per luminosity versus time.

(x) The current analysis was done assuming that  $\Upsilon(1S)$  are produced unpolarized. The acceptance variation due to the  $\Upsilon(1S)$  polarization is asymmetric, and depends on the  $\Upsilon(1S)$   $p_T$  and rapidity. It varies from -15% to +40% for the extreme cases of either pure longitudinal or transverse polarization. The variation is reduced to less than 4% when the  $\alpha$  parameter is restricted to within  $\pm 0.15$ . Our measurement of the  $\Upsilon(1S)$  polarization is in progress.

## VI. CONCLUSIONS

We presented a preliminary measurement of the inclusive production cross section of the  $\Upsilon(1S)$  bottomonium state using the  $\Upsilon(1S) \rightarrow \mu^+\mu^-$  decay mode. The data sample corresponds to an integrated luminosity of  $159.1 \pm 10.3$  pb $^{-1}$ . We determine differential cross sections as functions of the  $\Upsilon(1S)$  transverse momentum,  $p_T^{\Upsilon}$ , for three ranges of the  $\Upsilon(1S)$  rapidity:  $0 < |y^{\Upsilon}| < 0.6$ ,  $0.6 < |y^{\Upsilon}| < 1.2$ , and  $1.2 < |y^{\Upsilon}| < 1.8$ . The shapes of  $d\sigma/dp_T$  cross sections show

little variation with rapidity and are consistent with the published Run I CDF measurement over the rapidity range  $|y^T| < 0.4$ . The absolute cross sections integrated over  $p_T$  are also consistent with the published CDF results and exhibit rapidity dependence as expected from PYTHIA Monte Carlo. A comparison with other models of quarkonium production will follow.

### Acknowledgments

We thank the staffs at Fermilab and collaborating institutions, and acknowledge support from the Department of Energy and National Science Foundation (USA), Commissariat à L'Energie Atomique and CNRS/Institut National de Physique Nucléaire et de Physique des Particules (France), Ministry for Science and Technology and Ministry for Atomic Energy (Russia), CAPES, CNPq and FAPERJ (Brazil), Departments of Atomic Energy and Science and Education (India), Colciencias (Colombia), CONACyT (Mexico), Ministry of Education and KOSEF (Korea), CONICET and UBACyT (Argentina), The Foundation for Fundamental Research on Matter (The Netherlands), PPARC (United Kingdom), Ministry of Education (Czech Republic), Natural Sciences and Engineering Research Council and West-Grid Project (Canada), BMBF (Germany), A.P. Sloan Foundation, Civilian Research and Development Foundation, Research Corporation, Texas Advanced Research Program, and the Alexander von Humboldt Foundation.

- 
- [1] CDF Collaboration: F. Abe *et al.*, Phys. Rev. Lett. **69**, 3704 (1992); **79**, 572 (1997); **79**, 578 (1997).
  - [2] R. Baier, R. Ruckl, ZP **C19**, 251 (1983). M. Vanttinen *et al.*, Phys. Rev. D **D51**, 3332(1995); G. Schuler CERN-TH.7170/94
  - [3] H. Fritzsche, Phys. Letters 67B, 217(1977); R. Gavai *et al.*, IJ of MP A10, 3043(1995);  
J. Amundson *et al.*, Phys. Letters **B390**, 323 (1997);  
O. J. P. Eboli *et al.*, Phys. Rev. D **60**, 117501 (1999);  
C. B. Mariott, M. B. Ducati, G. Ingelman, hep-ph/0111379 (2001).
  - [4] A. Edin, G. Ingelman, J. Rathsman, Phys. Rev. D **56**, 7317 (1997).
  - [5] G. Bodwin, E. Braaten and G. Lepage, Phys. Rev. D **51**, 1125 (1995), Phys. Rev. D **55**, 5853 (1997); E. Braaten and S. Fleming, Phys. Lett. **74**, 3327 (1995); M. Cacciari *et al.*, Phys. Lett.**B356**, 553 (1995); P. Cho, A. Leibovitch, Phys. Rev. D **53** 150 (1996); 6203 (1996).
  - [6] E. L. Berger, J. Qiu and Y. Wang, hep-ph/0404158 preprint, May 2004.
  - [7] CDF Collaboration: F. Abe *et al.*, Phys. Rev. Lett.**75**, 4358 (1995).
  - [8] CDF Collaboration: T. Affolder *et al.*, Phys. Rev. Lett. **84**, 2094 (2000).
  - [9] CDF Collaboration: D. Acosta *et al.*, Phys. Rev. Lett. **88**, 161802 (2002).
  - [10] E. Braaten, S. Fleming and A. K. Leibovitch, Phys. Rev. D **63**, 094006 (2001).
  - [11] E Braaten and J. Lee, Phys. Rev. D **63**, 071501(R) (2001).
  - [12] C. N. Brown *et al.*, Phys. Rev. Lett. **86**, 2529 (2001).
  - [13] A. Zieminski, invited talk at the Charm Workshop, Trento, June 2002;  
[http://hep.physics.indiana.edu/~zieminsk/talks/trento\\_onia.ps](http://hep.physics.indiana.edu/~zieminsk/talks/trento_onia.ps).
  - [14] Particle Data Group; <http://pdg.lbl.gov>.
  - [15] T. Sjöstrand, L. Lönnblad, S. Mrenna and P. Skands, *PYTHIA 6.2*, hep-ph/0108264.

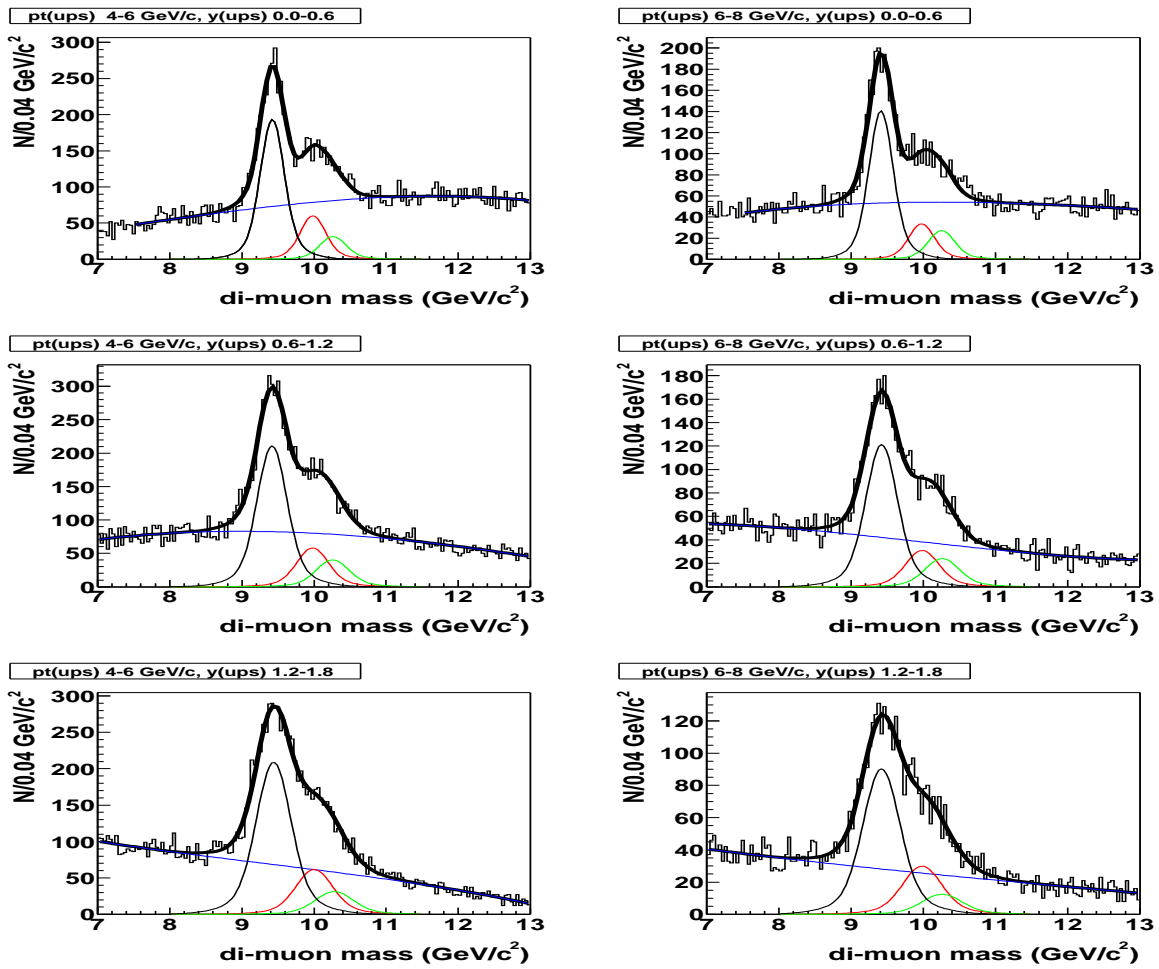


FIG. 1: Examples of the fits for the dimuon spectra in different bins of transverse momentum and rapidity. Both the SMT hit and isolation requirements were imposed.

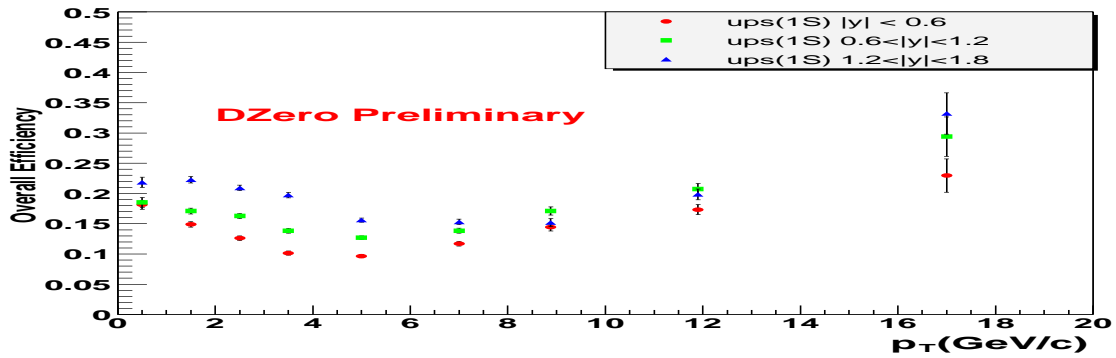


FIG. 2: Overall efficiency dependence on the  $\Upsilon(1S)$  transverse momentum, derived from Monte Carlo and trigger simulator, in three rapidity ranges. Data - Monte Carlo corrections are not included. Minima observed at medium  $p_T$  values are associated with the change in event topology.

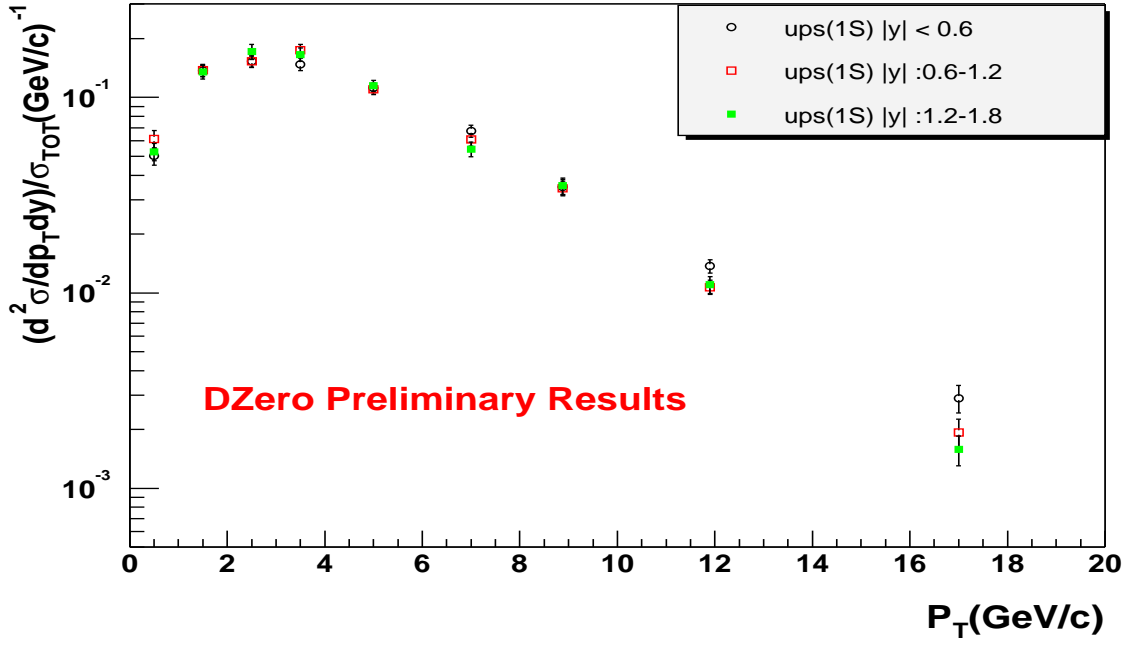


FIG. 3: Normalized differential cross sections for  $\Upsilon(1S)$  in different rapidity regions.

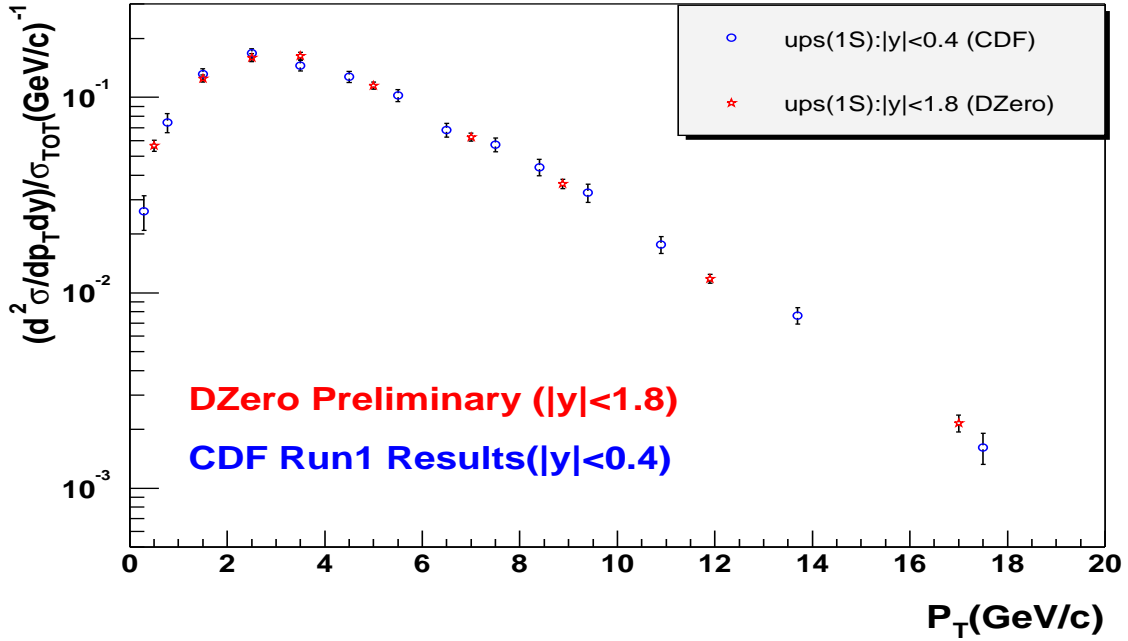


FIG. 4: Normalized differential cross sections for  $\Upsilon(1S)$  compared with the published CDF Run I results.

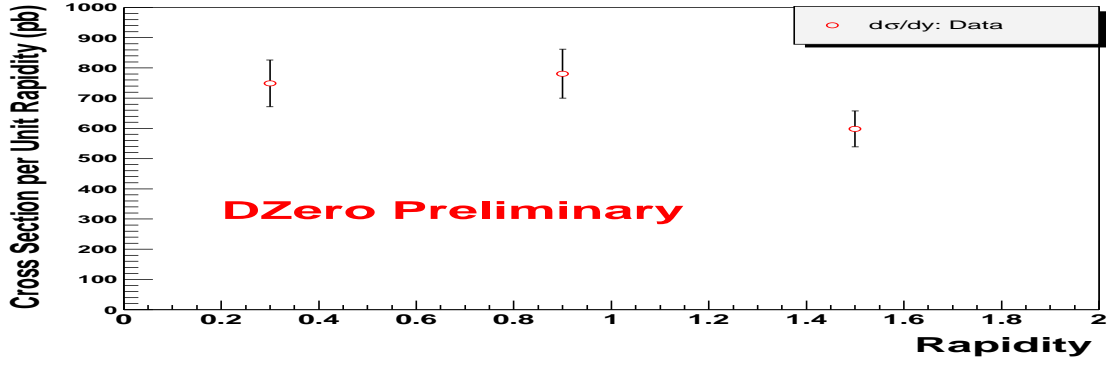


FIG. 5:  $\Upsilon(1S) \cdot B(\Upsilon(1S) \rightarrow \mu^+ \mu^-)$  production cross section per unit of rapidity as a function of rapidity. Data uncertainties are dominated by systematic effects.

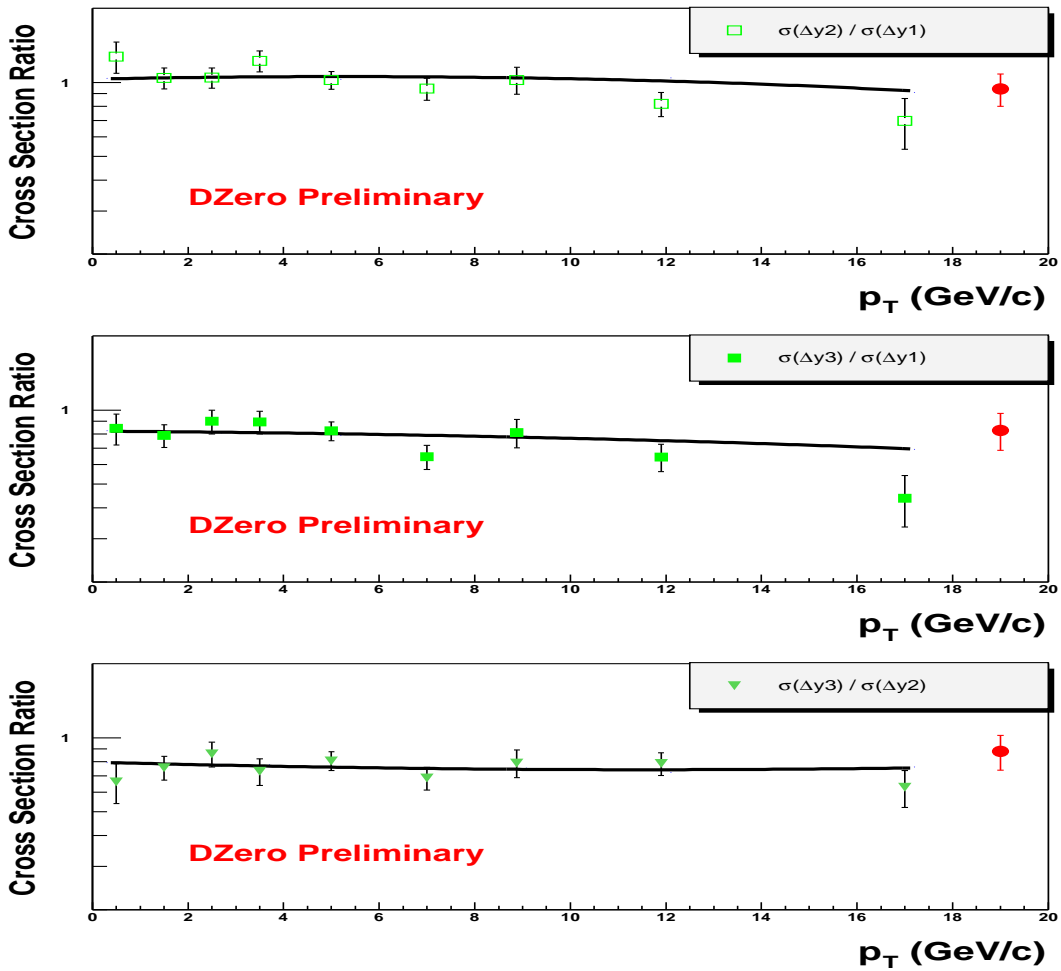


FIG. 6: Ratios of  $\Upsilon(1S)$  cross sections for different rapidities, plotted as a function of  $\Upsilon(1S)$  transverse momentum. PYTHIA Monte Carlo predictions are normalized to the measured ratios of the  $p_T$  integrated cross sections. Uncertainties of the relative normalization are also shown. They are plotted centered at a value predicted for a given ratio by PYTHIA.